







# Fires Following Earthquake Fragility Functions for Protected Steel Braced Frames

*Patrick Covi  and Nicola Tondini \*, Department of Civil, Environmental and Mechanical Engineering, University of Trento, Via Mesiano 77, 38123 Trento, Italy*

*Amir Sarreshtehdari  and Negar Elhami-Khorasani , Department of Civil, Structural and Environmental Engineering, University at Buffalo, Buffalo, NY 14260, USA*

**Received:** 2 April 2023/**Accepted:** 27 November 2023

**Abstract.** The paper describes the outcomes of the analysis of a steel braced frame protected with spray-applied fire resistive material and subjected to fires following earthquake (FFE). Nonlinear time-history analyses were performed in order to evaluate the seismic response. Then, the post-earthquake fire ignitions within selected compartments were considered based on the damage suffered by the structure, which was estimated according to the inter-storey drift ratio and floor acceleration. Natural fire curves were determined by means of zone models. Thus, compartmentation and opening characteristics were included in the analysis. Finally, thermomechanical analyses were completed and failure criteria based on the column and beam displacement and rate of displacement were investigated. The results of the probabilistic analyses were used to produce fragility functions to evaluate the probability of exceeding a limit state conditioned on an intensity measure in the context of FFE.

**Keywords:** Fire following earthquake, Fragility functions, Concentrically braced steel frames, Probabilistic framework, Spray-applied fire resistive material

## 1. Introduction

Structural engineering design generally considers seismic and fire loadings as two separate load cases. However, several historical events show that the consequences associated with fire following an earthquake (FFE) event can be significantly higher compared to the damages and losses caused by only the seismic event [1, 2]. The 1906 San Francisco earthquake was one of the most significant FFE scenarios, in which fires destroyed around 80% of the city. Other major FFE events that occurred in the past include the Tokyo earthquake (1923), in which fires destroyed 447,000 houses (38.3 km<sup>2</sup> burnt area) and 140,000 fatalities occurred [1, 2]. Fires after the Kobe earthquake (1995) destroyed 5000 buildings, and

---

\* Correspondence should be addressed to: Nicola Tondini, E-mail: [nicola.tondini@unitn.it](mailto:nicola.tondini@unitn.it)



fires were ignited after the Tohoku earthquake (2011) due to the earthquake itself or the tsunami caused by the seismic event [1, 2].

The major causes of post-earthquake ignitions in past earthquakes are reviewed by Botting [3]. Also, Scawthorn [4] discusses causes for ignition and predicts post-earthquake ignition rates for typical buildings for different earthquake intensities. In brief, the principal causes of ignition include overturning of electrical appliances, short-circuiting of electrical equipment, gas leakage from damaged equipment and pipework, and leakage of flammable fluids. Damaged gas equipment and pipes may cause sparks and contain fuel that could propagate the fire while electrical household appliances may initiate sparks involving interior furnishings and other flammable materials. Another major concern is the high potential for ignition as electricity and gas supplies are restored some time after the earthquake. Leaking gas and damaged electrical appliances were identified as initiating fires in the days following the Kobe and Northridge earthquakes.

An earthquake can lead to single or multiple ignitions in a building. In this context, the structural fire performance could deteriorate because the fire acts on a previously damaged structure. The earthquake may damage active and passive fire protection systems (e.g., sprinklers, compartmentation, insulation), leading to a faster fire spread and a more vulnerable structural system. Moreover, it is harder to control post-earthquake fires as there can be multiple ignitions across a community. The response of firefighters can be hampered due to earthquake damage to infrastructure networks, such as water (including its dependency on power), communication, and transportation [1]. Previous work studied the impacts of earthquake damage to transportation and water networks on the likelihood of fire spread across a community [5, 6].

A few works can be found on the post-earthquake behaviour of non-structural components, such as passive fire protection. For example, Braxtan et al. [7] performed a series of cyclic tests on sprayed fire-resistive material (SFRM) applied to steel members; the results of which indicated damage to the SFRM. Based on these outcomes, numerical analyses were carried out to investigate the post-earthquake fire response of a protected steel moment-resisting frame [8]. The post-earthquake fire performance of non-structural components was studied by the UCSD (University of California San Diego) [9, 10]. A shaking table test was carried out on a 5-storey reinforced concrete building to induce seismic damage, after which fires were ignited in different compartments. FFE tests on fire protected steel columns part of a steel-braced frame were conducted through a hybrid simulation technique by Covi et al. [11]. Considering the literature, there is a need to study the impact of earthquake damage to non-structural components on the fire response of the structure.

Fragility functions are convenient tools when decisions are to be taken in structural design considering uncertainties. They were extensively developed in the seismic engineering field [12–15] and a few researches have been made to derive fire fragility functions [16–21]. In greater detail, for a given structure exposed to earthquake or fire, a fragility function computes the probability that a structure reaches a predefined damage state (e.g. beam deflection level, interstorey drift ratio, critical temperature, etc.) depending on an intensity measure characterizing the haz-

ard, such as the seismic input (e.g. spectral acceleration at the fundamental period, peak ground acceleration) and the fire (e.g. fire load, fire geometry, etc.). Rare attempts at deriving FFE fragility functions can be found in the literature [22–24]. Based on the work [24], this paper extends the analysis by including the effect of the fire protections on the structural elements and by consequently computing the fragility functions for structural members. Moreover, a comparison between the outcomes of the unprotected and protected building is shown. Thus, it will focus on the consequences of fire ignitions inside a structure, with the objective to study post-earthquake fire performance of a protected steel braced frame considering uncertainties in the ground motions, fire behaviour, and material properties. Damage to structural and non-structural components is considered. The structural performance is characterized and presented in the form of fragility curves and surfaces.

## **2. FFE Framework**

The major steps for implementing the FFE probabilistic framework [25] are illustrated in Figure 1. The process is followed to perform probabilistic FFE analyses and to obtain sufficient data to build fragility curves and surfaces. The framework can be used to investigate structures with or without fire protection and it is developed and implemented using a combination of different software, i.e. OpenSees [26, 27], Ozone [28], and MATLAB [29]. The seismic analyses and the FFE structural analyses were performed in OpenSees. The zone model software Ozone [28] was used for the fire development analyses. It is not possible to automatically perform the thermal analyses inside OpenSees 3.2.0 [23–25]. For that reason, a specific code developed in MATLAB was exploited for the heat transfer analyses. The heat transfer MATLAB code is compatible with the Windows operating system and also Linux operating systems, typically used for High-Performance Computing (HPC) in order to reduce the computational burden. Alternatively, SAFIR [30] software can be used to perform the heat transfer analyses, noting that it is only compatible with the Windows operating system.

In detail, the geometry of the structural system, cross section sizes, material properties, and applied loads are first defined in a Tcl script (Step #1 of Figure 1). Probabilistic parameters required for the analysis, such as compartment properties, are next generated (Step #2). Once all the inputs and random variables are defined, the gravity and seismic analyses are performed (Step #3). Then, OpenSees enters a “standby mode” and a background MATLAB process executes the FFE decision algorithm to automatically generate fire ignitions and scenarios based on the seismic analysis results (Step #4), in which the temperature of the hot gases in the compartments is computed using Ozone (Step #5). Heat transfer is then conducted in SAFIR linked to MATLAB via text file input (Step 6), followed by the structural analysis at elevated temperatures in OpenSees (Step #7). Finally, the generated results are used to construct the fragility functions (Step #8).

The status of a compartment after an earthquake is based on the combined conditions of the glazing, partition walls, and doors and it is quantified using the

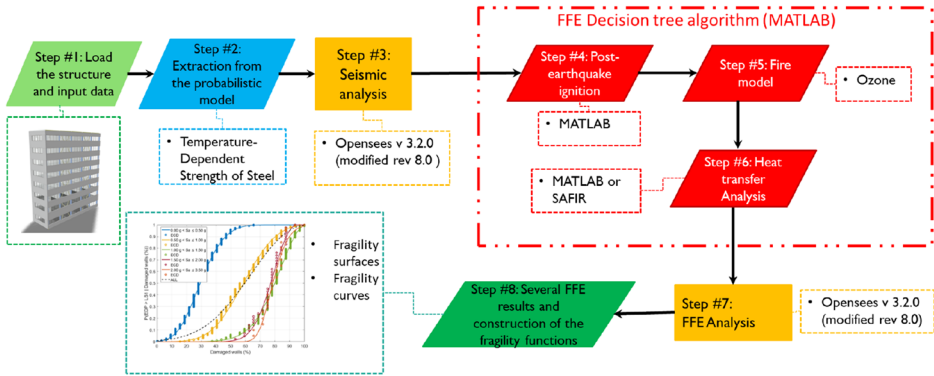


**Figure 1. Major steps in the implemented FFE framework.**

fragility functions provided in FEMA P58 [31] background documentation. After the earthquake, it is still challenging to precisely determine whether the doors are open or closed. As a result, the door status is associated with a random binary condition (open or closed) regardless of the magnitude of the earthquake. The framework determines the possible damage to each compartment (glazing and wall damages) and generates the fire scenario given the earthquake characteristics and using the following four thresholds:

- The horizontal peak floor acceleration (PFA) of at least one floor, which is a measure of the maximum acceleration experienced by a mass located on a given floor of the building during an earthquake, must be greater than or equal to 0.7 g, this value corresponds to the 100% probability of exceeding breakage in gas pipe joints according to the fragility curves reported in Ueno et al. [32].
- The inter-story drift ratio (IDR) of the same floor must be greater than or equal to 1.0%. This ignition criterion considers the possibility of having some damage to the electric cables that can be characterized as a function of the IDR. According to the FEMA P-356 [33], the requirements for life safety and collapse prevention performance levels for a steel braced frame structure are 0.5% and 2%, respectively. Therefore, the ignition criterion for a steel braced frame was assumed as 1% IDR, an arbitrary value in between the two thresholds.
- The maximum horizontal PFA of the building must be greater than or equal to 1.2 g, this value corresponds to the extensive damage state in sprinkler system components according to the fragility curves in the literature [34].
- The maximum IDR must remain below 6%. An IDR equal to 6% was chosen as the threshold for collapse, which is three times the recommended collapse limit state value for a braced steel frame (i.e., 2% IDR) in FEMA P-356 [33]. Extensive yielding, buckling of braces, and connection failure are expected during the earthquake without the subsequent FFE event.

The yield strength of steel  $f_y$  at ambient (seismic analysis) and high temperatures (fire analysis) was modelled as a random variable using a continuous logistic function [35, 36] (see Equation (1)).

$$k_{y,2\%,T} = \frac{1.7 \times \exp\left[\text{logit}\left(\widehat{k}_{y,2\%,T}^*\right) + 0.412 - 0.81 \times 10^{-3} \times T + 0.58 \times 10^{-6} \times T^{1.9} + 0.43 \times \varepsilon\right]}{\exp\left[\text{logit}\left(\widehat{k}_{y,2\%,T}^*\right) + 0.412 - 0.81 \times 10^{-3} \times T + 0.58 \times 10^{-6} \times T^{1.9} + 0.43 \times \varepsilon\right] + 1} \quad (1)$$

where  $\text{logit}\left(\widehat{k}_{y,2\%,T}^*\right) = \ln\left(\frac{\widehat{k}_{y,2\%,T}}{1 - \widehat{k}_{y,2\%,T}}\right)$ ,  $\widehat{k}_{y,2\%,T}^* = \frac{\widehat{k}_{y,2\%,T} + 10^{-6}}{1.7}$ , and  $\widehat{k}_{y,2\%,T}$  is the temperature-specific retention factor as prescribed by EN1993-1-2 [37].

A custom material class, i.e., SteelFFEThermal, was developed for nonlinear FFE analyses in OpenSees. The SteelFFEThermal material has the same definition as the Giuffrè-Menegotto-Pinto uniaxial steel stress–strain model at ambient temperature. However, when the temperature is applied, the material class switches the constitutive law to the stress–strain constitutive law for steel at elevated temperature as for EN 1993-1-2 [38]. Degradation in material strength and stiffness at increasing temperatures is represented by steel retention factors for yield strength, elastic modulus, and proportional limit, and the material constitutive law is defined according to EN 1993-1-2 stress–strain curve. A detailed explanation of the material class can be found in [25].

### 3. Case Study

An eight-story three-bay steel frame with concentric bracings in two central bays was selected as a case study, as illustrated in Figure 2. The structure is an office building designed and presented in NIST Technical Note 1863-2 [39]. The structural system is designed according to the ASCE 7-10 [40] recommendations for an area with high seismicity on the West Coast of the United States; in particular, the city of Los Angeles was chosen for the case study location.

The building has a rectangular plan of 46.33 m in the E–W direction, including five 9.14 m bays, and 31.01 m in the N–S direction, including five 6.10 m bays. The story height is 4.28 m with the exception of the first floor, which is 5.49 m high. In order to study different possible ventilation conditions, that could affect the gas temperature inside the compartment, the width of the windows of the building varied from 1.5–6 m (5–20 ft) with 1.5 m (5 ft) intervals, whilst the windows had a constant sill height of 1.2 m (4 ft).

Load combinations used for analysis are in accordance with ASCE 7 §2.3. The bracings are designed to withstand horizontal loads. Their participation in transferring gravitational loads to the foundation system is minimal. However, bracings provide lateral stiffness to the structure and may impact the response of beams/columns during thermal expansion/contraction in a fire event.

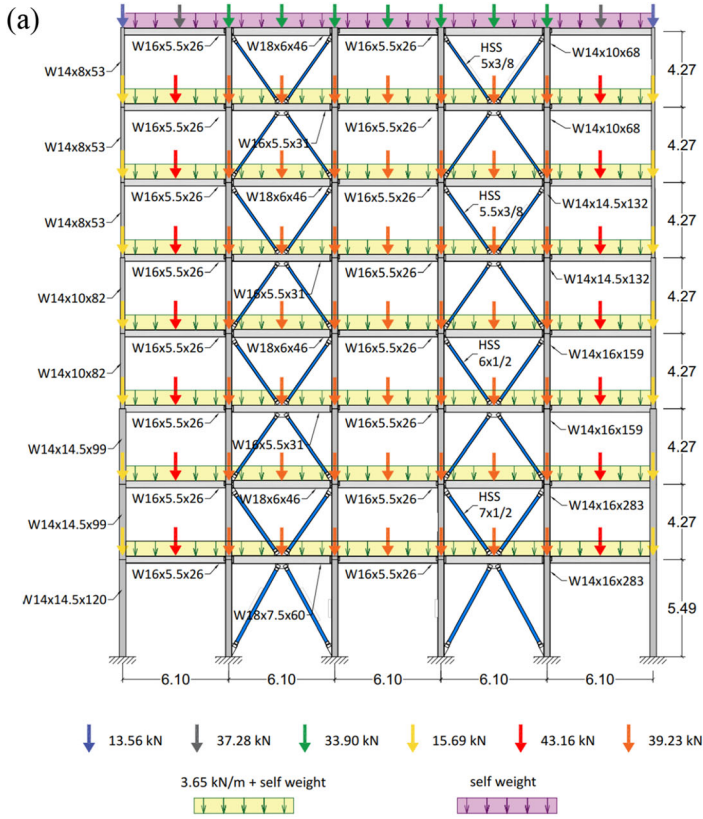


**Figure 2. (a) Configuration of the frame (lengths in meters); (b) example of render of the building.**

### **3.1. Ground Motions**

In order to perform non-linear time-history analyses, it was fundamental to model the seismic hazard through adequate selection and scaling of ground motion records. In this respect, a set of 14 accelerograms for the collapse limit state was selected from the FEMA P-695 dataset [41, 42] considering the type of spectrum, magnitude range, distance range, style-of-faulting, local site conditions, period range, and ground motion components using the PEER Ground Motion Database [43]. Table 1 summarizes the 14 strong motion records used for the N–S direction in the FFE analyses, including the magnitude and peak ground acceleration (PGA) and the same ID numbering given in FEMA P-695 [41]. The PGA is a measure of the maximum acceleration of the ground during an earthquake and it does not depend on the dynamic properties of the structure.

Accelerograms were modified to match the target spectrum in the period range of 0.3 s to 2.25 s that includes the fundamental period of the structure, which is equal to 1.5 s. Figure 3 illustrates the set of acceleration response spectra, original and scaled, and the scaled average response spectrum. The accelerograms were used to perform the FFE probabilistic analysis and 6 scale factors were applied to the accelerograms: 0.50; 0.75; 1.00; 1.25; 1.50; 1.75.

### **3.2. Design of the Passive Fire Protection**

The prototype structure presented in the NIST report was not originally designed against fire. However, based on the type of the building under consideration, the fire protection was designed to satisfy the fire requirements in accordance with the U.S. guidelines, including the 2021 International Building Code (IBC) [44] and AISC Design Guide 19 [45].

The required fire resistance rating is determined based on building features such as intended use and occupancy, construction material, building area, building height, fire department accessibility, distance from other buildings, sprinkler and smoke alarm system (see Table 2).

IBC Section 304 lists office buildings as Business Group B. The building classifies as construction Type IB based on IBC Table 503, and given the initial floor area (11,523 m<sup>2</sup>) and building height (35.4 m, 8 stories) without considering area or height increases. Structural steel framing is non-combustible and complies with the requirements of Type I and Type II construction.

IBC Table 601 requires a 2-h fire resistance rating for the structural frame of this building. In high-rise buildings, special requirements for automatic sprinklers allow for replacing Type IB with Type IIA requirements, which implies a 1-h reduction in the fire resistance rating for both the columns and floors. Thus, the required fire resistance rating for the case study is 1 h.

Commonly used insulation materials include insulation boards, intumescent paint, and spray-applied fire-resistive materials (SFRM). For this case study, passive fire protection made of spray-based vermiculite [46, 47] applied to the steel structural members was selected. The SFRM thickness can be determined using the IBC equation, a direct reference to a test (i.e., UL Certified product), or an equation listed in the test listings.

**Table 1**  
**Accelerogram Set for the Non-linear Time-History Analyses**

ID	Event name	Station	Year	Mw	PGA (g)
1	Northridge, USA	Beverly Hills—Mulhol	1994	6.7	0.52
2	Northridge, USA	Canyon Country-WLC	1994	6.7	0.48
3	Duzce, Turkey	Bolu	1999	7.1	0.82
5	Imperial Valley, USA	Delta	1979	6.5	0.35
6	Imperial Valley, USA	El Centro Array #11	1979	6.5	0.38
8	Kobe, Japan	Shin-Osaka	1995	6.9	0.24
9	Kocaeli, Turkey	Duzce	1999	7.5	0.36
10	Kocaeli, Turkey	Acelik	1999	7.5	0.22
11	Landers, USA	Yermo fire station	1992	7.3	0.24
14	Loma Prieta, USA	Gilroy Array #3	1989	6.9	0.56
16	Superstition Hills, USA	El Centro Imp. Co	1987	6.5	0.36
17	Superstition Hills, USA	Poe road (temp)	1987	6.5	0.45
18	Cape Mendocino, USA	Rio Dell overpass	1992	7	0.55
19	Chi-Chi, Taiwan	CHY101	1999	7.6	0.44

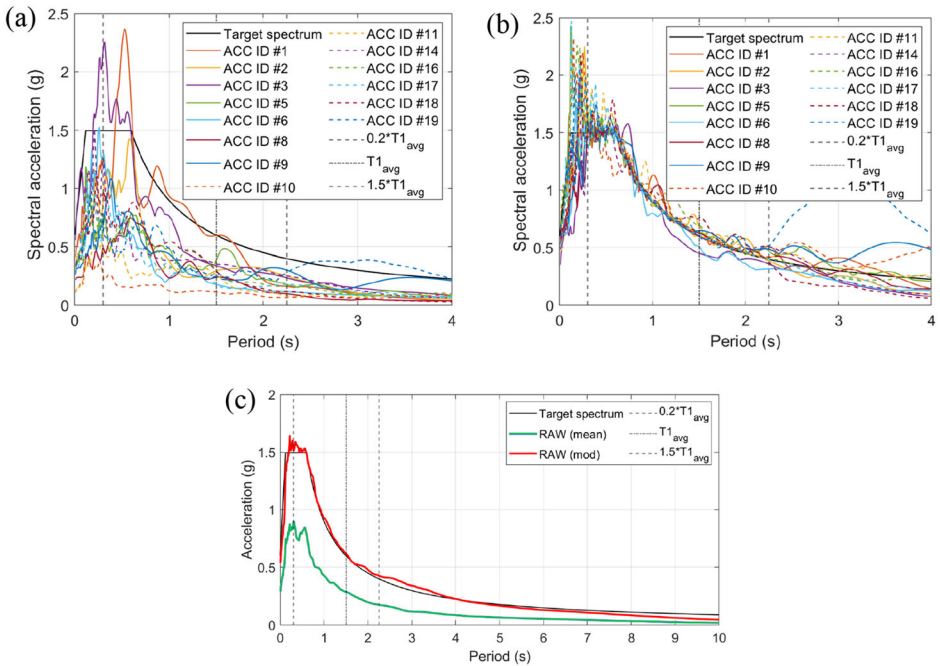


**Figure 3. Acceleration Response Spectra: (a) original, (b) scaled, (c) scaled average spectrum.**



**Table 2**  
**Building Features to Determine Fire Resistance Rating**

Occupancy	Office building
Height	35.4 m (116 ft)
Height of highest occupied floor	31.1 m (102 ft)
Footprint	1440 m <sup>2</sup> (152 ft×102 ft = 15,504 sq ft)
Total area	11,523 m <sup>2</sup> (15,504×8=124,032 sq ft)
Building perimeter	77.4 m (254 ft)
Active fire protection	Automatic sprinkler
Material combustibility	Non-combustible construction

Based on UL Certified product [46], the required thickness of the SFRM to be applied to all surfaces of the steel columns for all rating periods may be determined from the following equations:

$$h = \frac{R}{75\left(\frac{W}{D}\right) + 32} \quad (2)$$

where:

- h = SFRM thickness in the range of 1/4 in. to 4-1/2 in. (rounded up to the nearest 1/16 in.).
- R = Fire resistance rating period in minutes (60–240 min.).
- D = Heated perimeter of the steel column in inches.
- W = Weight of the steel column in lbs per foot.

According to the UL Certified [46] product information, the required thickness of SFRM to be applied to all surfaces of the steel pipe or steel tube for all rating periods may be determined from:

$$h = \frac{R}{188\left(\frac{A}{P}\right) + 45} \quad (3)$$

where:

- h = SFRM thickness in the range of 5/16 in. to 4-1/4 in. (rounded up to the nearest 1/16 in.).
- R = Fire resistance rating in minutes (60–240 min.).
- A = Cross-sectional area of pipe or tube.
- P = Heated perimeter of steel pipe or tube.

The beams used in the fire test will seldom match the steel sections used in the actual building. However, the thickness of SFRM applied to the test beam can be

used as a basis for calculating the thickness to be used on the substitute beam [47]. The equation for adjusting the SFRM thickness of the tested beam is:

$$T_1 = \frac{\left(\frac{W_2}{D_2} + 0.6\right) T_2}{\frac{W_1}{D_1} + 0.6} \quad (4)$$

where:

- T = Thickness (in.) of spray-applied material.
- W = Weight of beam (lb/ft).
- D = Perimeter of protection, at the interface of the fire-protection material and the steel through which heat is transferred to steel (in.).
- Subscript 1 = Refers to alternate beam size and required material thickness.
- Subscript 2 = Refers to given beam size and material thickness shown in the individual designs.

Based on these formulas, the required SFRM thickness for each structural member is shown in Table 3.

### 3.3. Fire Loads

The fire load was systematically sampled as it may affect the fire scenario and consequently the structural response. Based on a discrete uniform sampling, five values of fire load density were selected: i.e., 300 MJ/m<sup>2</sup>; 600 MJ/m<sup>2</sup>; 900 MJ/m<sup>2</sup>; 1200 MJ/m<sup>2</sup>; 1500 MJ/m<sup>2</sup>. In the EN 1991-1-2 [37], an 80% fractile value of fire load density for office occupancies corresponds to 511 MJ/m<sup>2</sup> according to the Gumbel distribution. According to a recent survey conducted in the US, the measured total fire load density, including moveable and fixed content, had a mean value of 1486 MJ/m<sup>2</sup> [48]. For this reason, fire load density values up to 1500 MJ/m<sup>2</sup> were used and fire load density less than 300 MJ/m<sup>2</sup> was considered too low.

### 3.4. Finite Element Model

The 3D frame was modelled with non-linear beam elements based on corotational formulation and the uniaxial SteelFFEThermal material was used for the braces, beams and columns. Equivalent geometric imperfections were included for columns and braces to allow for geometric imperfections, e.g., member out-of-straightness, and mechanical imperfections, such as residual stresses. The magnitude of such imperfections was selected according to EN 1993-1-1 [49]. Masses were considered lumped at the floors. The thickness of the slab (3 1/4 in = 83 mm) was such that in the seismic analysis the floors behave as rigid diaphragms in their plane. A sensitivity analysis was performed in order to determine the mesh size of the elements to obtain adequate precision in the calculation of displacements, stresses, and strains in sections of each member. As a result, four beam elements for the column, eight elements for the beam, and eight elements for bracings were

**Table 3**  
**SFRM Thickness**

Columns	W/D	h (inches) (rounded up to the nearest 1/16 in.)	h (mm)
W14 × 68	1.02	9/16	14.3
W14 × 132	1.54	7/16	11.1
W14 × 159	1.76	3/8	9.5
W14 × 283	2.98	1/4	6.4
W14 × 53	0.91	5/8	15.9
W14 × 82	1.22	1/2	12.7
W14 × 99	1.18	1/2	12.7
W14 × 120	1.41	1/2	12.7

Braces	A/P	h (inches) (rounded up to the nearest 1/16 in.)	h (mm)
HSS 5 × 5 × 3/8	0.31	5/8	15.9
HSS 5.5 × 5.5 × 3/8	0.31	5/8	15.9
HSS 6 × 6 × 1/2	0.41	1/2	12.7
HSS 7 × 7 × 1/2	0.41	1/2	12.7

Beams	W/D	T <sub>1</sub> (inches) (rounded up to the nearest 1/16 in.)	T <sub>1</sub> (mm)
W16 × 26	0.56	1/2	12.7
W18 × 46	0.87	3/8	9.5
W16 × 31	0.66	7/16	11.1
W18 × 60	1.04	5/16	8.0

considered, respectively. An equivalent damping ratio of 3% was assumed for the seismic simulations.

In order to reduce the computational time to perform thousands of FFE analyses, the full 3D model of the building (including the secondary frame and the full slab) was not considered in this work. It is worth pointing out that the slab is not composite with the beams and consequently its effect would be minor. Nonetheless, the slab (which acts as a heat sink) was considered when performing the thermal analysis.

## **4. Probabilistic Analysis Results**

### **4.1. Earthquake Simulation**

For brevity, one sample simulation is selected as an example to demonstrate the methodology used for the FFE analyses. The selected seismic action is shown in Figure 4. The earthquake, known as the Imperial Valley earthquake, occurred at 4:16 pm, October 15, 1979 with a magnitude of 6.5.

Figure 5 illustrates the results of the numerical simulation of the non-linear dynamic analysis for the selected acceleration time-history. The energy dissipation

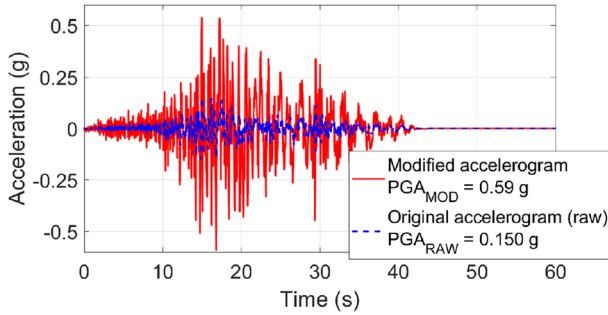


**Figure 4. Comparison between the original and modified accelerogram for the Imperial Valley ground motion.**

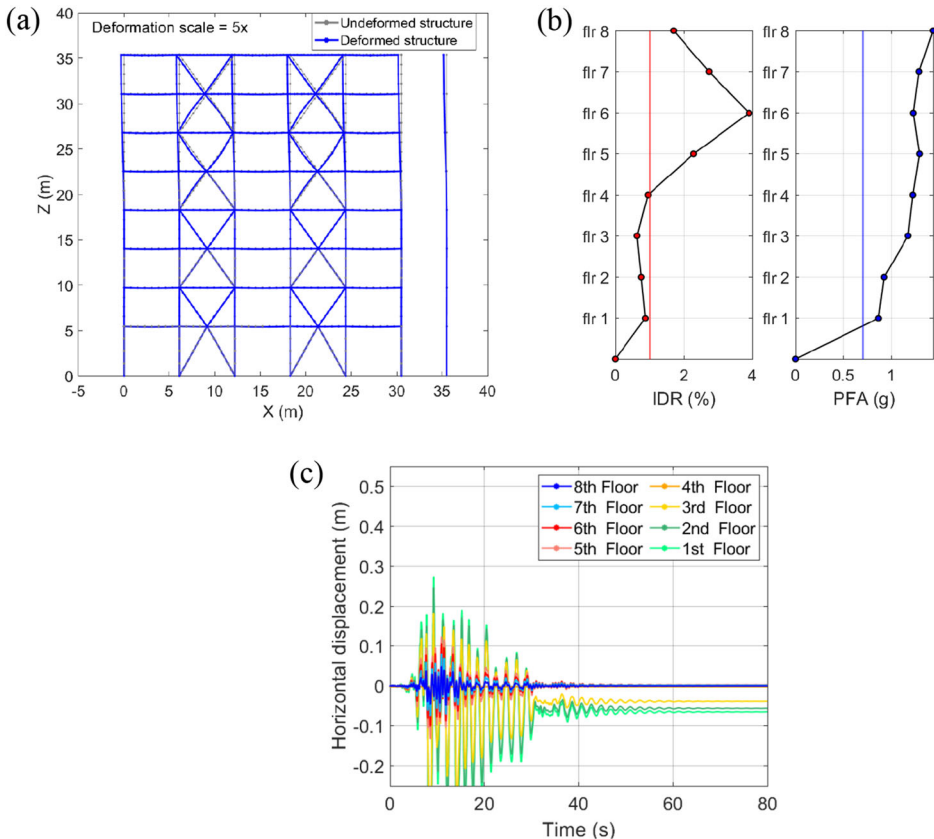


**Figure 5. (a) Deformed shape at the end of the seismic event (amplified by a factor of 5); (b) maximum inter-story drift (IDR) and maximum peak floor acceleration (PFA); (c) horizontal displacement of the floors.**

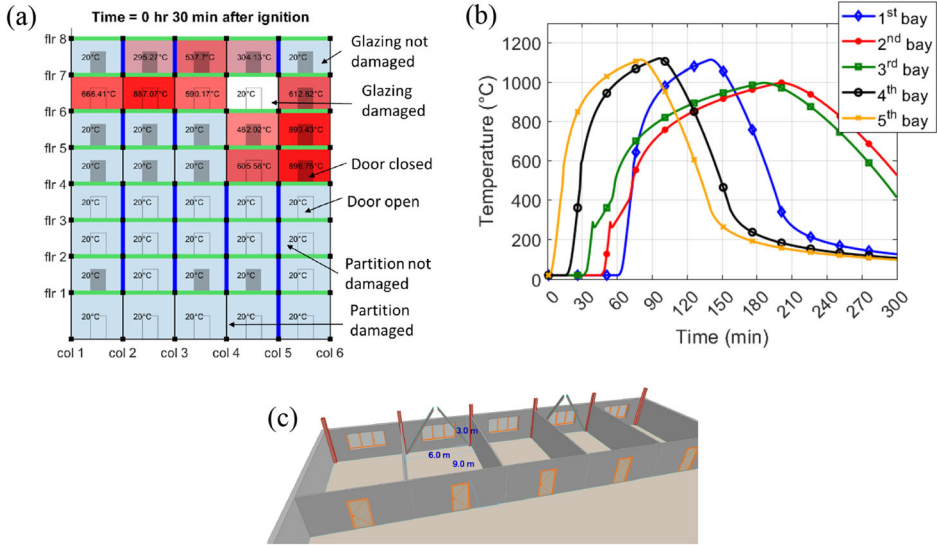


**Figure 6. (a) Fire spread within the building after 30 min; (b) time-temperature curve of fire for floor 5; (c) inside view of a compartment.**

was concentrated in the braces. This means that the energy introduced by the earthquake was dissipated by cyclic inelastic behavior of the braces. Thus, the seismic damage was located in the bracing system, whereas beams and columns were designed to remain elastic to avoid low dissipation mechanisms in the context of the capacity design philosophy.

#### 4.2. Post-earthquake Fire Simulation

The probabilistic FFE framework was used to automatically determine the possible damage to each compartment (glazing and wall damages) and generate the fire scenario based on the IDR and PFA thresholds. The framework includes the possibility to have the ignition in more than one compartment due to multiple damage to the gas or electrical services or appliances in more than one location. For this reason, the framework could select more than one ignition after the earthquake. The flashover time is set as the threshold for the vertical spread between two exterior compartments. The horizontal fire spread rate in the Grenfell Tower fire incident was about 0.3 m/min [50]. Bailey et al. [51] assumed a 36 min delay between the ignition of two adjacent 8-m bays in a building. Therefore, in the direction of the horizontal compartments, a delay time of 30 min or 15 min was taken for the horizontal fire spread, depending on whether or not the partition remains intact after the earthquake event [52]. Figure 6a shows the evolution of the fire for a sample FFE scenario, Figure 6b illustrates the time-temperature curves for each compartment on the 5th floor, while Figure 6c shows a qualitative

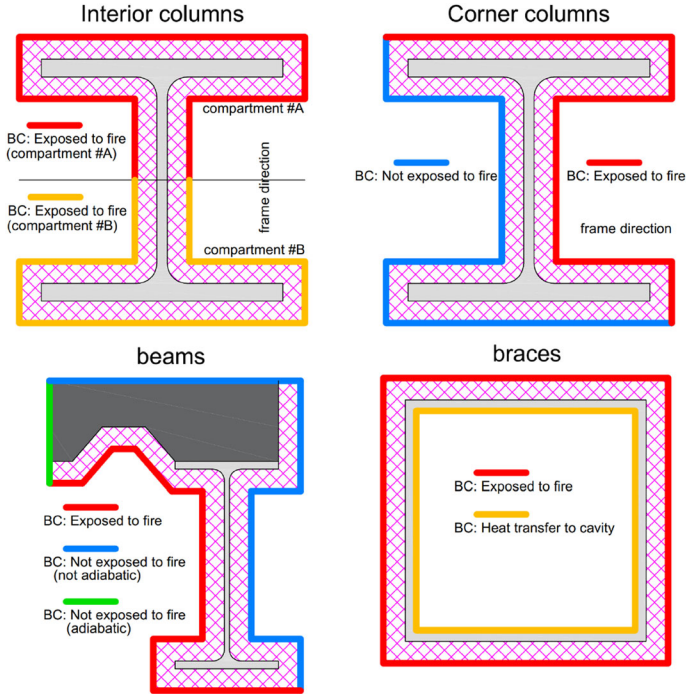


**Figure 7. Boundary conditions for thermal analysis.**

representation of the compartment locations and dimensions for the selected case study.

Once ignition locations are determined based on the established thresholds on IDR and PFA, generated temperature–time curves by Ozone are assigned to the compartments considering the values for fire load and ventilation in a given iteration. The fire spread inside the building is then tracked based on the assigned vertical and horizontal fire spread rates. The heat transfer analysis was automatically performed to obtain steel temperatures for each element in the compartment subjected to fire using the probabilistic FFE framework. Figure 7 shows the boundary conditions for the heat transfer analyses of the columns, braces, and beams taken for the case study under consideration. These boundary conditions are typical of perimeter frames.

The density ( $\rho_i$ ), thermal conductivity ( $k_i$ ), and specific heat ( $c_i$ ) of SFRM at high temperatures (thermal analysis) was modelled using the probabilistic models [35] (see Equations (5), (6), (7)) by taking the median value, i.e.  $\varepsilon = 0$ , and  $T$  in  $^{\circ}\text{C}$  as shown in Figure 8. Previous sensitivity studies indicated that the density and specific heat of SFRM can be treated as deterministic [17]. The uncertainty in thermal conductivity should ideally be incorporated in the analysis; however, considering the number of random variables in the FFE framework, the thermal conductivity of the SFRM is modeled as a deterministic parameter to keep the computational cost manageable.

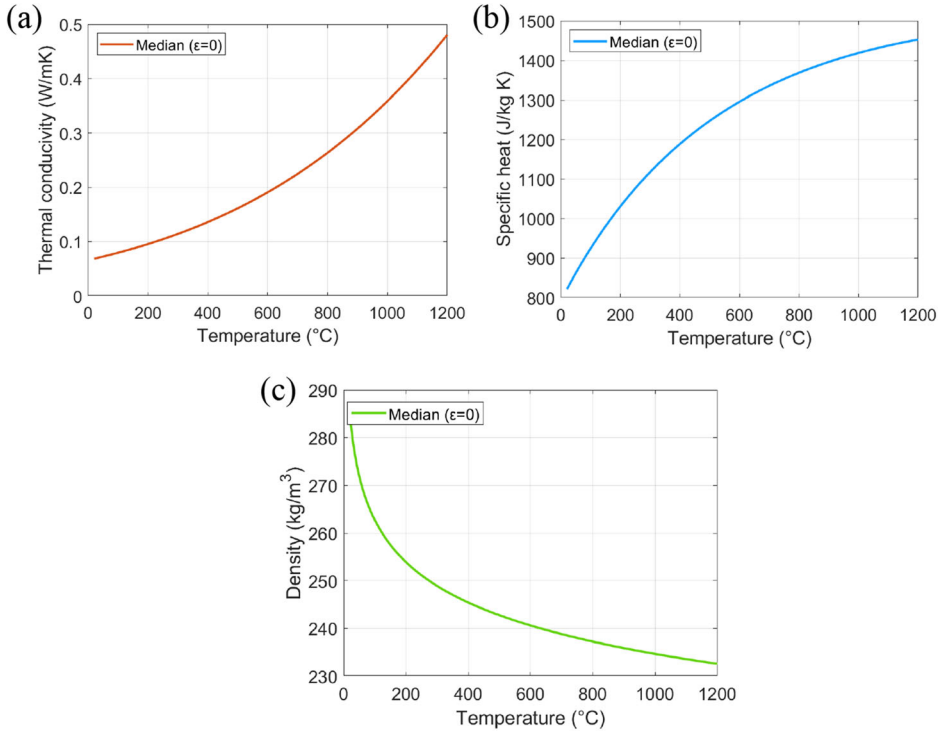


**Figure 8. Thermal properties of spray-applied fire resistive material: (a) thermal conductivity; (b) specific heat; (c) density.**

$$k_i = \exp(-2.72 + 1.89 \times 10^{-3}T - 0.195 \times 10^{-6}T^2 + 0.209 \times \varepsilon) \quad (5)$$

$$c_i = 1700 - \exp(6.81 - 1.61 \times 10^{-3}T + 0.44 \times 10^{-6}T^2 + 0.213 \times \varepsilon) \quad (6)$$

$$\rho_i = \exp(-2.028 + 7.83 \times T^{-0.0065} + 0.122 \times \varepsilon) \quad (7)$$

The thermal field in the cross section is generally defined in OpenSees at multiple temperature zones and up to 15 zones for 3D beam-column elements, as shown in Figure 9b, d. Thus, the Matlab script extracts 15 temperature data zones from the thermal analyses and generates the input data for OpenSees. The concrete slab was considered only for the thermal analyses. Also, the insulation material has only thermal properties without any mechanical resistance.

The FFE structural analysis followed the heat transfer analysis for the selected scenario. Partial structural collapse occurred 62 min after the start of the fire due to the excessive rate of vertical deflection in the beams located on the 5th and 6th floors and in the 5st bay, as illustrated in Figure 10a.

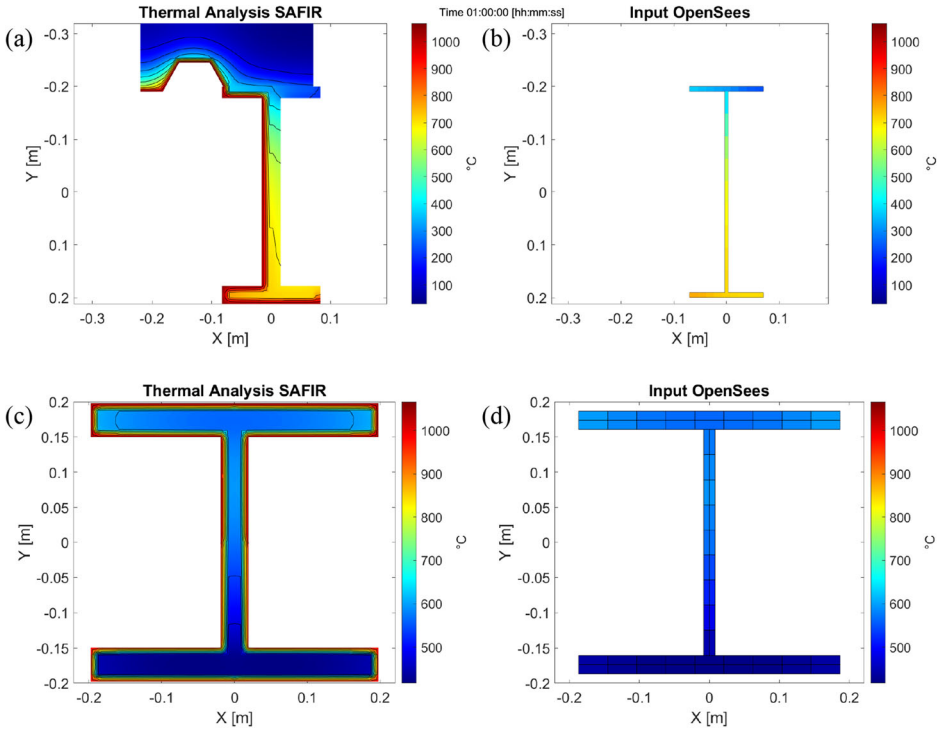


**Figure 9. Temperature distribution of structural elements in the compartment at floor 5 - bay 5 (a) W14 14.5 132 beam (Safir thermal model); (b) W14 14.5 132 beam (Equivalent OpenSees); (c) W16 5.5 26 column (Safir thermal model); (d) W16 5.5 26 column (Equivalent OpenSees).**

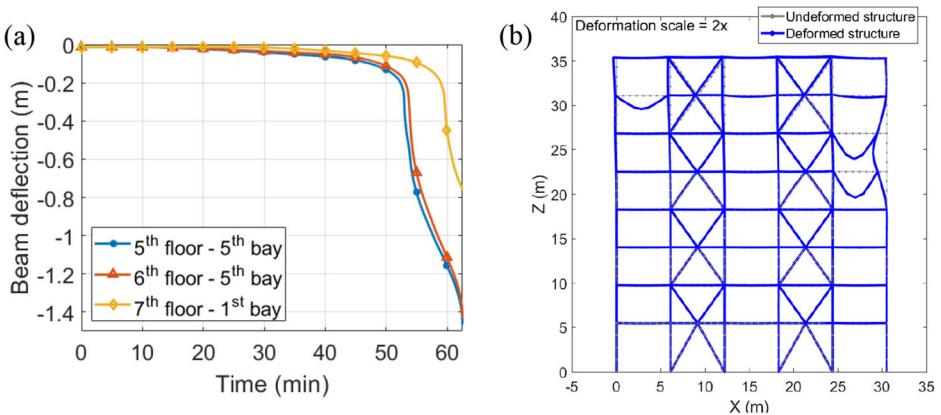


**Figure 10. (a) Beams deflection (b) deformed shape after 62 min (partial structural collapse).**



**Table 4**  
**Analysis Parameters for the FFE Analysis**

Parameter	Values
Accelerograms	14 accelerograms
Acceleration scale factor	0.50, 0.75, 1.00, 1.25, 1.50 1.75
Window width (m)	1.5, 3.0, 4.5, 6.0
Fire load density (MJ/m <sup>2</sup> )	300, 600, 900, 1200, 1500

Figure 10b shows the final deformed configuration of the steel frame at the end of the simulation. In particular, despite the low utilization factor of the columns, the loss of transverse restraint owing to the beam failure caused an increase in the column effective length that eventually led to column buckling and the collapse of a portion of the building.

### 4.3. Results

A total of 1680 simulations were performed for 14 accelerograms scaled at 6 different intensity values, 4 different values of window width, and 5 different fire load densities, as listed in Table 4. Scaling is applied to the records as a uniform scale factor. Scaling of the natural ground motions is often needed and it is a common practice in performance-based seismic engineering applications to induce large nonlinear behaviour, because a few high-intensity earthquake events have been recorded [53]. The Latin Hypercube Sampling (LHS) [54] was used to randomly generate the variable  $\varepsilon$  for steel retention factor  $k_{y,2\%,T}$ , which was needed to calculate the yield strength at ambient and high-temperatures for each simulation using Equation (1).

The simulation results were classified into several categories as shown in Figure 11 and listed below:

- Structure collapsed due to earthquake: The collapse of the building due to the seismic event is related to the likelihood of extensive damage to the structural elements, which can be characterized by the inter-story drift ratio. As previously mentioned, an IDR equal to 6% was chosen as the threshold for collapse, which is three times the recommended collapse limit state value for a braced steel frame (i.e., 2% IDR) in FEMA P-356 [33]. Extensive yielding, buckling of braces, and connection failures are expected at the selected threshold. Thus, simulations with maximum inter-story drift ratios larger than 6% were considered to experience structural collapse during the earthquake without the subsequent FFE analysis (232 out of 1680 analyses).
- No FFE event: No FFE occurred because the thresholds for IDR and PFA were not exceeded for an ignition to happen (277/1680 analyses).
- FFE event — the structure safeguarded by sprinkler system: The FFE event started and the sprinkler system remained functional after the earthquake event. The fire was successfully extinguished by the sprinkler system without

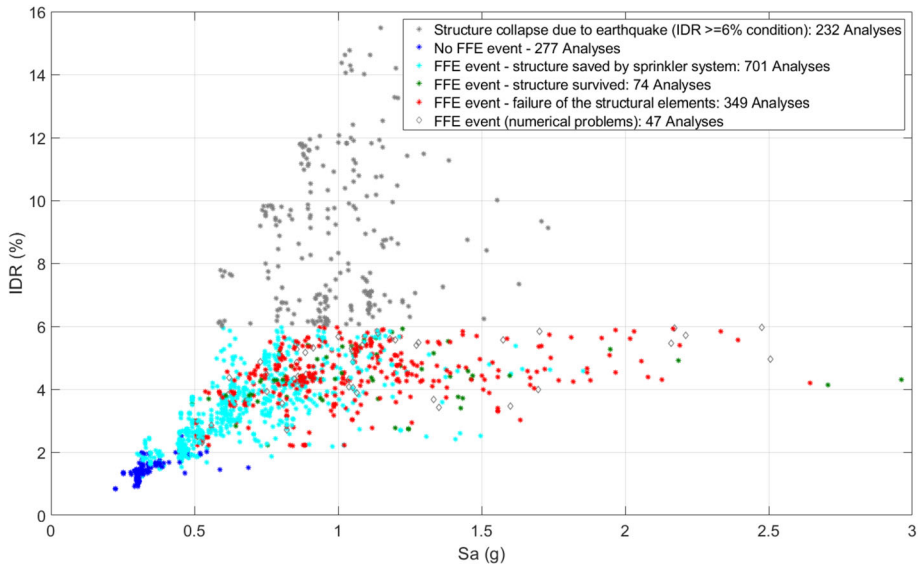


**Figure 11. Classification of the analysis results.**

any partial/total collapse of the structure or failure of structural elements (701/1680 analyses).

- FFE event — the structure survived: The FFE event started, sprinklers and active firefighting measures to extinguish the fire were not functional after the earthquake (as previously mentioned, a PFA equal to 1.20 g was chosen as the threshold). The structure survived the FFE event without any partial/total collapse of the structure and without any failure of the structural elements (74/1680 analyses).
- FFE event — partial/total collapse of the structure or failure of the structural elements: The FFE event occurred, sprinklers and active firefighting measures to extinguish the fire were not functional after the earthquake. At least one element reached the failure limit state (349/1680 analyses).
- “FFE event — numerical problems: The FFE event started but the analysis was interrupted due to numerical problems before reaching the beam or column failure limit state. These simulations were discarded in the analysis of results (47/1680 analyses).

Figure 11 shows the maximum IDR as a function of the spectral acceleration (Sa) at the first period of the structure, where the results are grouped based on the above-mentioned classifications. The spectral acceleration is a measure of the maximum acceleration experienced by a damped harmonic oscillator in an earthquake event.

Figure 12a shows the number of ignitions as a function of the maximum Sa at the first period of the structure. It can be observed that for larger values of Sa the

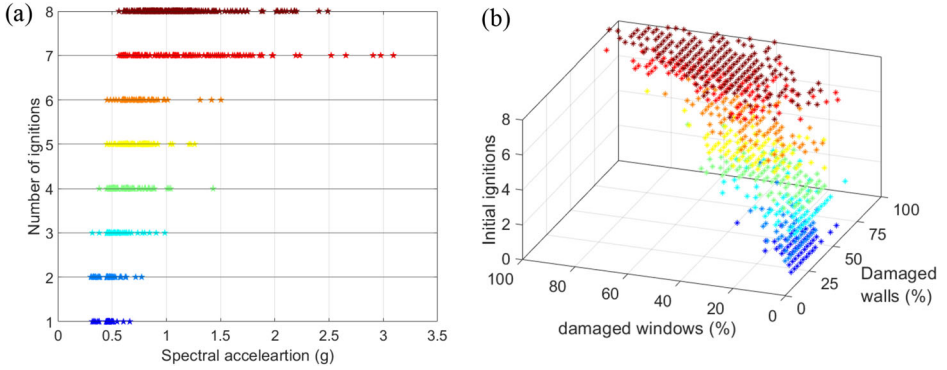


**Figure 12. (a) Number of ignitions vs  $S_a$ ; (b) Number of ignitions vs damaged windows and walls.**

number of ignitions is higher. Figure 12b shows the number of ignitions as a function of the percentage of damaged walls and windows after the earthquake event.

## 5. Fragility Functions

### 5.1. Methodology

FFE fragility functions were developed based on the results of the simulations. As mentioned in the Introduction, a fragility function expresses the probability  $P$  of a given engineering demand parameter (EDP), such as IDR exceeding a certain limit state (LS) conditioned on an intensity measure (IM), such as peak ground acceleration or fire load density. Fragility functions are often expressed in terms of a log-normal cumulative distribution and have the form of Equation (8).

$$P(EDP > LS | IM = x) = \Phi \left( \frac{\ln \left( \frac{x}{\theta} \right)}{\beta} \right) \quad (8)$$

where  $\Phi$  is the standard normal cumulative distribution function (CDF),  $\theta$  is the median of the IM and  $\beta$  is the standard deviation of the intensity measure. A typical EDP representing the damage induced by a seismic event is IDR, whereas in the case of an FFE, meaningful EDPs as related to structural fire engineering are vertical or horizontal displacements and displacement rates of structural members. A representative IM for an FFE scenario is the time to failure of a structural member that reflects the level of damage induced by the earthquake. Many researchers studied statistical procedures for estimating parameters of fragility functions and characterizing the results of probabilistic models, especially in the seismic domain [14, 15, 55] but also in the fire domain [17, 18, 20, 56]. Although the EDP is commonly assumed to follow a lognormal distribution when condi-

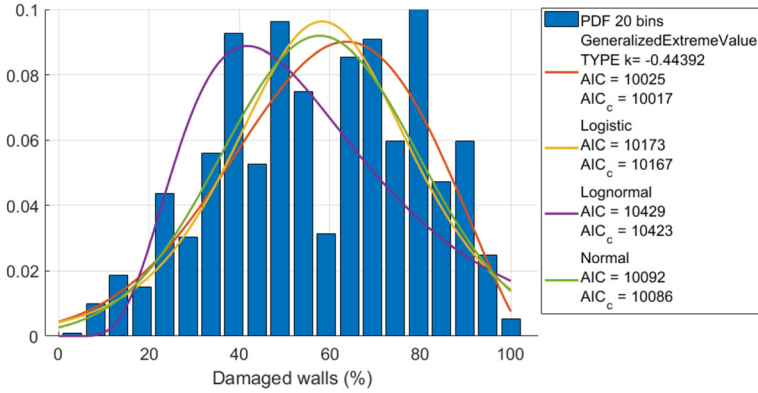


**Figure 13. Probability density function (PDF) of the damaged walls and function distributions.**

tioned on the IM, several other distributions were considered and compared using the Akaike information criterion (AIC) method [57, 58], as illustrated in Figure 13. Equation (9) illustrates the AIC mathematical method, which evaluates and compares different possible statistical models and determines which one fits the data best.

$$AIC = -2\ln L + 2k \tag{9}$$

where  $L$  and  $\ln L$  are respectively the likelihood and the log-likelihood at its maximum point of the estimated model and  $k$  is the number of parameters. The use of a second-order corrected AIC ( $AIC_c$ ) is recommended when the sample size is small compared to the number of parameters ( $n/k < 40$ ) [59], as shown in Equation (10):

$$AIC_c = AIC + \frac{2k^2 + 2k}{n - k - 1} \tag{10}$$

where  $n$  denotes the sample size. Note that for  $n \rightarrow \infty, AIC_c = AIC$ .

AIC uses a model’s maximum likelihood estimation (log-likelihood) as a measure of fit and adds a penalty term for models with higher parameter complexity to avoid overfitting. Given a set of candidate models for the data, the preferred model is the one with the minimum AIC value.

The outcome of comparing the performance of different probability density functions (PDFs) for the generated FFE data is illustrated in Figure 13. The results in Figure 13 indicate that compared to other statistical models, the lognormal distribution can serve as a candidate distribution to define the FFE fragility function. However, the Generalized Extreme Value (GEV) distribution showed the best fit to the data.

Based on the results of the comparative analysis, the GEV distribution was selected to derive the fragility functions. Not only the distribution provides the

best fit, but also can be represented in a simple and closed form function with three parameters. The cumulative distribution function for the GEV distribution has the form of Equation (11).

$$P(EDP > LS | IM = x) = \begin{cases} \exp\left\{-\left[1 + k\left(\frac{x-\mu}{\sigma}\right)\right]^{-1/k}\right\} & \text{if } k \neq 0 \\ \exp\left\{-\exp\left[-\left(\frac{x-\mu}{\sigma}\right)\right]\right\} & \text{if } k = 0 \end{cases} \quad (11)$$

where  $\sigma$  denotes the scale parameter (statistical dispersion of the probability distribution),  $\mu$  is the location parameter (shift of the distribution), and  $k$  is the shape parameter. The shape parameter  $k$  is used to represent three different distribution families (Gumbel distribution, Fréchet distribution, reversed Weibull distribution).

### 5.2. Fragility Functions for Non-structural Components

Fragility functions for non-structural components are here derived. The shape value  $k$  is always below 0 for the case study analysed in this work (see Table 3). Thus, the GEV Type III was used for the fragility functions. This distribution is equivalent to the reversed Weibull distribution, whose tails are finite, such as the beta distribution (Table 5).

Figure 14a, b show the fragility curves for the damaged walls and are grouped as a function of the  $S_a$  at the first period of the structure, respectively, using the GEV and Lognormal distribution. As expected, the Generalized Extreme Value (GEV) distribution showed a better fit to the data compared to the lognormal distribution. It may be noted that the higher the spectral acceleration the larger the initial percentage of damaged walls.

### 5.3. Fragility Functions for Structural Members

Different limit states, following EN 1363-1 [60], are defined to identify failure in the structural members:

**Table 5**  
**Parameters of the GEV and Lognormal Distributions for the Fragility Functions of Damaged Walls Grouped Based on  $S_a$**

	GEV distribution			Lognormal distribution	
	$k$	$\sigma$	$\mu$	$\sigma$	$\mu$
0.0 g < $S_a$ ≤ 0.5 g	- 0.209	11.89	25.26	0.492	3.306
0.5 g < $S_a$ ≤ 1.0 g	- 0.300	16.78	52.93	0.313	4.028
1.0 g < $S_a$ ≤ 1.5 g	- 0.535	13.78	75.37	0.183	4.345
1.5 g < $S_a$ ≤ 2.0 g	- 0.456	9.903	73.85	0.129	4.327
2.0 g < $S_a$ ≤ 3.5 g	- 0.166	7.400	76.03	0.102	4.367

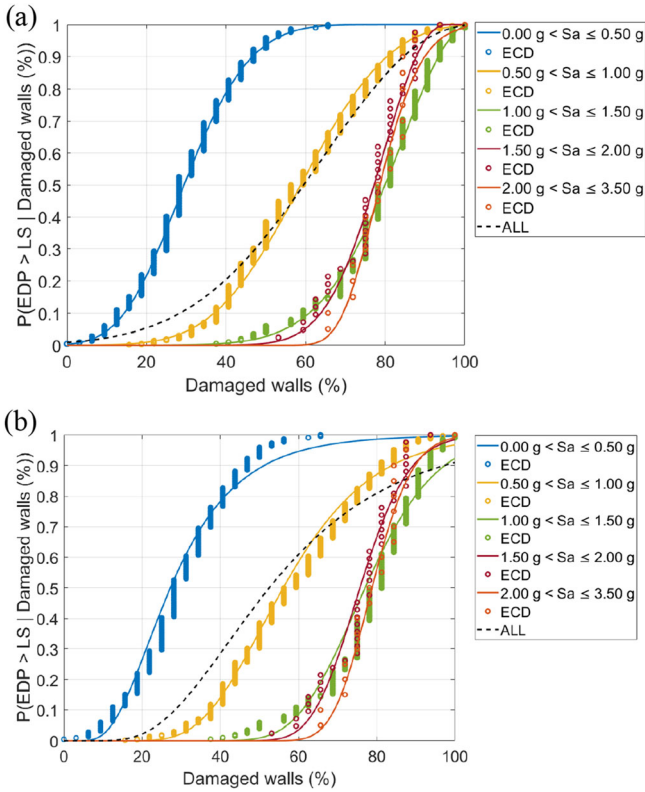


**Figure 14. Empirical cumulative distribution (ECD) and fragility curves for the damaged walls as a function of  $S_a$ ; (a): GEV distribution, (b) Lognormal distribution.**

- Beams—Limit state 1 (LS1):

- (i) deflection exceeding  $L^2/400d$
- (ii) rate of deflection exceeding  $L^2/(9000d)$  mm/min

- Columns—Limit state 2 (LS2):

- (i) vertical contraction exceeding  $C = h/100$  mm
- (ii) rate of vertical contraction exceeding  $dC/dt = 3$  h/1000 mm/min

Despite the fact that LS1 and LS2 are derived from the standard fire tests, they provide a measure about the extent of damage that the structural members may undergo.

Another limit state based on [17] was considered for the column that corresponds to a sudden increase in transversal deflection.

● Columns—Limit state 3 (LS3):

(i) rate of lateral deflection at mid-height 50 mm/min

where  $h$  is the initial column height in mm,  $L$  is the beam length, and  $d$  is the depth of the beam. It is worth pointing out that failure of a column may lead to the partial or global collapse of the building based on the degree of redundancy, whereas failure of a beam may not be as critical as a column failure.

In every FFE scenario of the case study presented in this paper, the beam always fails before the column, as shown in Figure 15a. The difference in the median of the failure time for the beam and the first column that follows the beam failure is about 15 min. The column failure does not necessarily occur in the same compartment where the beam fails. Figure 15b shows the fragility curves for the probability of exceedance of reaching the beam limit state as a function of the fire load density and time to failure. No element failures or partial collapse were observed in FFE scenarios with a fire load value of 300 MJ/m<sup>2</sup>, because no fire scenario was able to induce gas temperatures high enough and/or long enough to cause failure of a protected beam or column. For all other fire loads, the beam failure condition was reached. The median and standard deviation of the failure time for all fire load density values equal to or greater than 600 MJ/m<sup>2</sup> are 53 min and 10 min. It should be noted that selecting a sufficient measure of the hazard to develop the fragility curves requires attention to the characteristics of the hazard. A combination of fire load density and time to failure is selected to ensure that the effect of fire scenario (short-duration high-temperature fire versus long-duration low-temperature fire) is captured on the structural response.

Figure 16a, b show the fragility curves and surfaces, respectively, for the beam failure conditioned on the time to failure and grouped as a function of the  $S_a$  at the first period of the structure. Figure 16a illustrates different slices of Figure 16b.

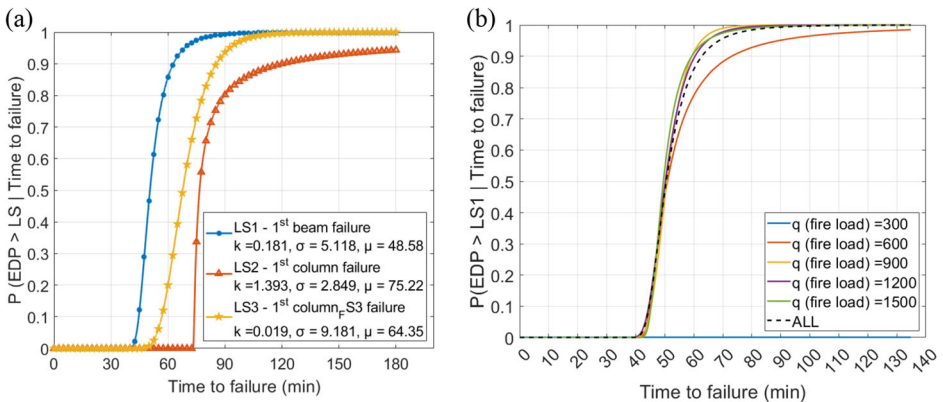


**Figure 15. (a) Comparison of the beam and column failure times; (b) Fragility curves for the beam limit state as a function of the fire load density.**

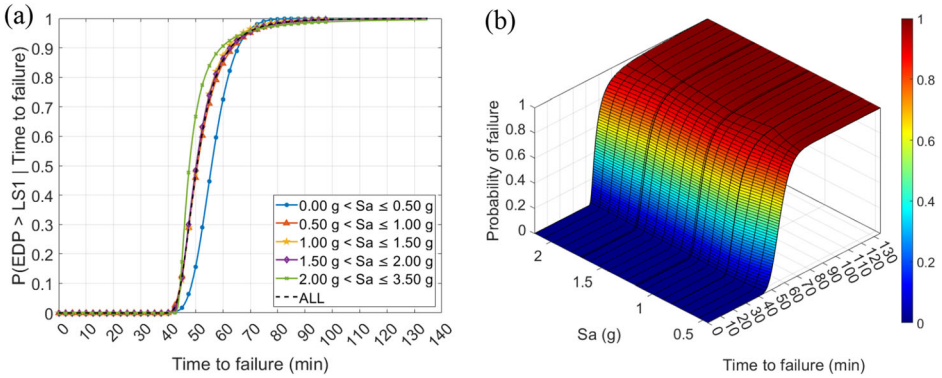


**Figure 16. (a) Fragility curves for the beam limit state as a function of  $Sa$ ; (b) fragility surface for the beam limit state as a function of  $Sa$ .**

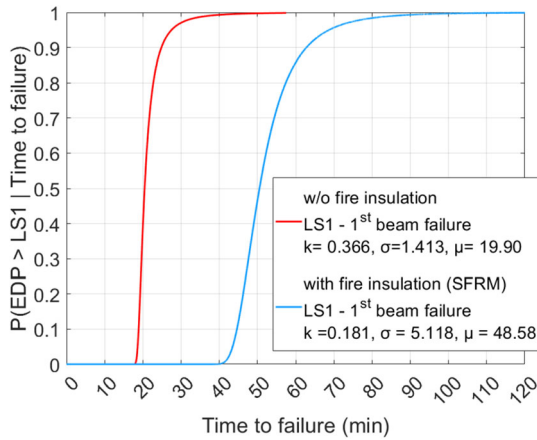


**Figure 17. Comparison of the beam failure times with and without fire protection (SFRM).**

An earthquake event could extensively damage the active and passive fire protections, which would have a significant impact on the structural fire performance. It is expected that fire protection at locations of plastic hinges experiences more damage compared to non-dissipative members [61, 62]. However, for a steel braced frame, no plastic hinges are expected owing to a seismic event and inelastic behaviour of the braces occurs, but their damage may not be critical for the structural collapse under FFE scenarios. Indeed, this was shown in previous work performed on the same steel braced frame but unprotected [23]. In fact, a conservative approach could be to not model the fire protection considering the likelihood of damage to the passive fire protection during an earthquake. Figure 17 compares the results of this paper and the results of the same structure without fire protection presented in previous work [23]. Figure 17 highlights a



higher probability of exceedance of reaching the beam failure limit state with shorter times to failure when the structure is not protected. There is a 90% probability of exceeding the beam failure limit state in 25 min for the unprotected case, whereas the beam failure limit state for the protected case is reached in 62 min for the same target probability. The protected structure has a larger dispersion for beam failure time, ranging from 42 to 100 min. It is worth pointing out that in case of partial damage to the fire protections, the fragility curve would be in between the two curves shown in Figure 17.

## **6. Conclusions**

The paper presented a methodology to perform fire following earthquake (FEE) analyses and described the development of a novel probabilistic FFE framework aimed at developing FFE fragility functions of a prototype steel braced frame protected with spray-applied fire resistive material (SFRM). A decision tree algorithm was developed to establish the probability of ignition in the compartments within the building after the seismic event. Compartmentation and opening characteristics as well as the potential for fire spread were considered based on seismic damage in windows, doors, partition walls, and sprinkler system following seismic fragility functions found in the literature.

The results showed that about 1123 analyses, out of 1680 randomly generated cases, experienced FFE events and the structure was safeguarded by the sprinkler system in 701 analyses out of 1123 FFE events. The results of the probabilistic analyses were used to produce fragility functions to evaluate the probability of exceeding a damaged state conditioned on an intensity measure in the context of FFE. A higher probability of exceedance of reaching the collapse limit state with shorter times to collapse was observed when the structure was subjected to higher values of spectral acceleration. Moreover, higher values of the spectral acceleration led to a higher number of ignitions.

In cases with FFE, beams were always the first element to fail and the median value of time to reach the beam limit state was about 53 min for the structure protected with SFRM and 20 min for the unprotected structure. The fire load density had a significant impact on the failure time. No element failures or partial collapse were observed for a fire load of 300 MJ/m<sup>2</sup> in all FFE simulations, because no fire scenario was able to induce gas temperatures high enough and/or long enough to cause failure of a protected structural member.

This study provided some insights into the performance of protected concentrically steel framed buildings subjected to earthquake and fire. Future research can include other types of unprotected and protected steel structures, e.g., other braced and moment-resisting frames, as well as partial damage to passive fire protection from the earthquake.

## **Acknowledgements**

The research leading to these results has received funding from the Italian Ministry of Education, Universities and Research (MIUR) in the framework of the project DICAM-EXC (Departments of Excellence 2023-2027, grant L232/2016).

Computational support was provided by the Center for Computational Research at the University at Buffalo [63].

## **Funding**

Open access funding provided by Università degli Studi di Trento within the CRUI-CARE Agreement. This work was funded by Ministero dell'Istruzione, dell'Università e della Ricerca (Grant No.: L 232/2016).

## **Data Availability**

Some or all data, models, or codes that support the findings of this study are available from the corresponding author upon reasonable request.

## **Open Access**

This article is licensed under a Creative Commons Attribution 4.0 International License, which permits use, sharing, adaptation, distribution and reproduction in any medium or format, as long as you give appropriate credit to the original author(s) and the source, provide a link to the Creative Commons licence, and indicate if changes were made. The images or other third party material in this article are included in the article's Creative Commons licence, unless indicated otherwise in a credit line to the material. If material is not included in the article's Creative Commons licence and your intended use is not permitted by statutory regulation or exceeds the permitted use, you will need to obtain permission directly from the copyright holder. To view a copy of this licence, visit <http://creativecommons.org/licenses/by/4.0/>.

## **References**

1. Scawthorn C, Eidinger JM, Schiff AJ (2005) Fire following earthquake. Technical Council on Lifeline Earthquake Engineering Monograph, No. 26. American Society of Civil Engineers
2. Elhami-Khorasani N, Garlock MEM (2017) Overview of fire following earthquake: historical events and community responses. *Int J Dis Resil Built Environ* . [10.1108/IJDRBE-02-2015-0005](https://doi.org/10.1108/IJDRBE-02-2015-0005)
3. Botting R (1998). The Impact of Post-Earthquake Fire on the Built Urban Environment. Fire Engineering Research Report 98/1, University of Canterbury, New Zealand.

## *Fires Following Earthquake Fragility Functions*

4. Scawthorn CR, Khater M (1992). Fire following Earthquake: Conflagration Potential in the in greater Los Angeles, San Francisco, Seattle and Memphis Areas, EQE International, prepared for the National Disaster Coalition, San Francisco, CA (available from the National Committee on Property Insurance, 75 Tremont, Suite 510, Boston, MA 02108–3910, (617. 722–0200)).
5. Sarreshtehdari A, Elhami Khorasani N (2022) Post-earthquake emergency response time to locations of fire ignitions. *J Earthq Eng* 26(7):3389–3416. [10.1080/13632469.2020.1802369](https://doi.org/10.1080/13632469.2020.1802369)
6. Coar M, Sarreshtehdari A, Garlock M, Elhami Khorasani N (2021) Methodology and challenges of fire following earthquake analysis: an urban community study considering water and transportation networks. *Nat Hazards* . [10.1007/s11069-021-04795-6](https://doi.org/10.1007/s11069-021-04795-6)
7. Braxtan NL, Pessiki SP (2011) Postearthquake fire performance of sprayed fire-resistive material on steel moment frames. *J Struct Eng* 137(9):946–953
8. Keller WJ, Pessiki SP (2012) Effect of earthquake-induced damage to spray-applied fire-resistive insulation on the response of steel moment-frame beam-column connections during fire exposure. *J Fire Prot Eng* 22(4):271–299
9. Meacham BJ (2016) Post-earthquake fire performance of buildings: summary of a large-scale experiment and conceptual framework for integrated performance-based seismic and fire design. *Fire Technol* 52(4):1133–1157
10. Pantoli E, Chen M, Wang X, Astroza R, Ebrahimian H, Hutchinson T, Faghihi M (2016) Full-scale structural and nonstructural building system performance during earthquakes: part II—NCS damage states. *Earthq Spectra* 32(2):771–794
11. Covi P, Tondini N, Korzen M, Lamperti Tornaghi M (2023) Hybrid fire following earthquake tests on fire protected steel columns, IFireSS 2023—International Fire Safety Symposium—Rio de Janeiro, Brazil.
12. Mackie KR, Stojadinović B (2005). Comparison of incremental dynamic, cloud, and stripe methods for computing probabilistic seismic demand models. In *Structures Congress 2005: Metropolis and Beyond* (pp. 1–11).
13. Gardoni P, Der Kiureghian A, Mosalam KM (2002) Probabilistic capacity models and fragility estimates for reinforced concrete columns based on experimental observations. *J Eng Mech* 128(10):1024–1038
14. Baker JW (2015) Efficient analytical fragility function fitting using dynamic structural analysis. *Earthq Spectra* 31(1):579–599
15. Tondini N, Zanon G, Pucinotti R, Di Filippo R, Bursi OS (2018) Seismic performance and fragility functions of a 3D steel-concrete composite structure made of high-strength steel. *Eng Struct* 174:373–383
16. Gernay T, Elhami-Khorasani N, Garlock M (2016) Fire fragility curves for steel buildings in a community context: a methodology. *Eng Struct* 113:259–276
17. Gernay T, Khorasani NE, Garlock M (2019) Fire fragility functions for steel frame buildings: sensitivity analysis and reliability framework. *Fire Technol* 55:1175–1210
18. Lange D, Devaney S, Usmani A (2014) An application of the PEER performance based earthquake engineering framework to structures in fire. *Eng Struct* 66:100–115
19. Shrivastava M, Abu AK, Dhakal RP, Moss PJ (2019) Severity measures and stripe analysis for probabilistic structural fire engineering. *Fire Technol* 55:1147–1173
20. Randaxhe J, Popa N, Vassart O, Tondini N (2021) Development of a plug-and-play fire protection system for steel columns. *Fire Saf J* 121:103272
21. Possidente L, Randaxhe J, Tondini N (2023) Fire fragility curves for industrial steel pipe-racks integrating demand and capacity uncertainties. *Fire Technol* 59(2):713–742
22. Memari M, Mahmoud H (2018) Framework for a performance-based analysis of fires following earthquakes. *Eng Struct* 171:794–805

23. Covi P, Tondini N, Elhami-Khorasani N, Sarreshtehdari A (2023) Development of a novel fire following earthquake probabilistic framework applied to a steel braced frame. *Struct Saf* . [10.1016/j.strusafe.2023.102377](https://doi.org/10.1016/j.strusafe.2023.102377)
24. Covi P, Tondini N, Elhami-Khorasani N, Sarreshtehdari A (2022) Fires following earthquake fragility functions of steel braced frames, *SiF 2022—12th International Conference on Structures in Fire*, Hong Kong.
25. Covi, P. (2021). Multi-hazard analysis of steel structures subjected to fire following earthquake. Doctoral dissertation, University of Trento. [https://doi.org/10.15168/11572\\_313383](https://doi.org/10.15168/11572_313383)
26. McKenna F (2011) Opensees: a framework for earthquake engineering simulation. *Comput Sci Eng* 13(4):58–66
27. Elhami-Khorasani N, Garlock ME, Quiel SE (2015) Modeling steel structures in opensees: enhancements for fire and multi-hazard probabilistic analyses. *Comput Struct* 157:218–231
28. Cadorn JF, Franssen JM (2003) A tool to design steel elements submitted to compartment fires—OZone V2. Part 1: pre-and post-flashover compartment fire model. *Fire Safety Journal* 38(5):395–427
29. MATLAB Release 2021b (2021), The MathWorks Inc, Natick, Massachusetts
30. Franssen J-M, Gernay T (2017) Modeling structures in fire with SAFIR: theoretical background and capabilities. *J Struct Fire Eng* 8(3):300–323
31. Federal Emergency Management Agency (FEMA). (2012) Next-Generation Methodology for Seismic Performance Assessment of Buildings. Prepared by the Applied Technology Council for the Federal Emergency Management Agency, Report No. FEMA P-58, Washington, D.C.
32. Ueno J, Takada S, Ogawa Y, Matsumoto M, Fujita S, Has-sani N, Ardakani FS, (2004) Research and development on fragility of components for the gas distribution system in greater Tehran, Iran, *Conference Proceedings*, in Proc. 13th WCEE, Vancouver, BCCanada, Paper, no. 193.
33. FEMA (2000) Prestandard and commentary for the seismic rehabilitation of buildings
34. Soroushian S, Maragakis E, Zaghi AE, Echevarria A, Tian Y, Filiatrault A (2014). Comprehensive analytical seismic fragility of fire sprinkler piping systems (Vol. 14). MCEER.
35. Elhami-Khorasani N, Gardoni P, Garlock M (2015) Probabilistic fire analysis: material models and evaluation of steel structural members. *J Struct Eng* 141:12
36. Qureshi R, Ni S, Elhami-Khorasani N, Van Coile R, Hopkin D, Gernay T (2020) Probabilistic models for temperature-dependent strength of steel and concrete. *J Struct Eng* 146(6):04020102
37. CEN (2002): EN 1991–1–2 Eurocode 1: Actions on structures - Part 1–2: General actions - Actions on structures exposed to fire.
38. CEN (2005): EN 1993–1–2 “Eurocode 3: Design of steel structures - Part 1–2: General rules - Structural fire design”.
39. Harris JL, Speicher MS (2015) “Assessment of first generation performance-based seismic design methods for new steel buildings”. volume 2: special concentrically braced frames. (national institute of standards and technology). NIST Technical Note 2:1863–1872
40. ASCE 7-10 (2010). Minimum design loads for buildings and other structures. American Society of Civil Engineers.[34] ASCE 7-10 (2010). Minimum design loads for buildings and other structures. American Society of Civil Engineers.
41. Federal Emergency Management Agency (FEMA) (2008) FEMA P-695, Quantification of Building Seismic Performance Factors
42. Kircher C, Deierlein G, Hooper J, Krawinkler H, Mahin S, Shing B, Wallace J (2010). Evaluation of the fema p-695 methodology for quantification of building seismic performance factors

## *Fires Following Earthquake Fragility Functions*

43. Ancheta TD, Darragh RB, Stewart JP, Seyhan E, Silva WJ, Chiou BSJ, Wooddell KE, Graves RW, Kottke AR, Boore DM, Kishida T, Do-nahue JL (2013) PEER NGA-West2 Database, PEER 2013/03
44. International Code Council. (2020) International building code. In: International Code Council.
45. American Institute of steel construction (2003) AISC DESIGN GUIDE 19
46. UL Product iQ, BXUV.X845 - Fire-resistance Ratings - ANSI/UL 263. <https://iq.ulprospector.com/en/profile?e=15514>
47. UL Product iQ, BXUV.D795 - Fire-resistance Ratings - ANSI/UL 263. <https://iq.ulprospector.com/en/profile?e=13815>
48. Elhami-Khorasani N, Salado Castillo JG, Saula E, Josephs T, Nurlybekova G, Gernay T (2021) Application of a digitized fuel load surveying methodology to office buildings. *Fire Technol* . [10.1007/s10694-020-00990-2](https://doi.org/10.1007/s10694-020-00990-2)
49. CEN (2005): EN 1993-1-1 Eurocode 3: Design of steel structures - Part 1-1: General rules and rules for buildings
50. Guillaume E, Drean V, Girardin B, Benameur F, Fateh T (2020) Reconstruction of grenfell tower fire. Part 1: lessons from observations and determination of work hypotheses. *Fire Mater* 44(1):3–14
51. Bailey CG, Burgess IW, Plank RJ (1996) Analyses of the effects of cooling and fire spread on steel-framed buildings. *Fire Saf J* 26(4):273–293
52. Sarreshtehdari A, Elhami Khorasani N (2021) Integrating the fire department response within a fire following earthquake framework for application in urban areas. *Fire Saf J* 124:103397
53. Tothong P, Luco N (2007) Probabilistic seismic demand analysis using advanced ground motion intensity measures. *Earthq Eng Struct Dynam* 36(13):1837–1860
54. Olsson A, Sandberg G, Dahlblom O (2003) On Latin hypercube sampling for structural reliability analysis. *Struct Saf* 25(1):47–68
55. Calvi GM, Pinho R, Magenes G, Bommer JJ, Restrepo-Vélez LF, Crowley H (2006) Development of seismic vulnerability assessment methodologies over the past 30 years. *ISET J Earthq Technol* 43:75–104
56. Randaxhe J, Popa N, Tondini N (2021) Probabilistic fire demand model for steel pipe-racks exposed to localised fires. *Eng Struct* 226:111310
57. Akaike H (1998) Information theory and an extension of the maximum likelihood principle. *Selected papers of hirotugu akaike* Springer, New York, pp 199–213
58. Akaike H (1974) A new look at the statistical model identification. *IEEE Trans Autom Control* 19(6):716–723
59. Burnham KP, Anderson DR (1998) Practical use of the information-theoretic approach. *Model selection and inference* Springer, New York, pp 75–117
60. EN 1363-1 (2020): Fire resistance tests - Part 1: General requirements
61. Braxtan NL, Pessiki SP (2011) Postearthquake fire performance of sprayedfire-resistive material on steel moment frames. *J Struct Eng* 137(9):946–953
62. Lamperti Tornaghi M, Tsionis G, Pegon P, Molina J, Peroni M, Korzen M, Tondini N, Covi P, Abbiati G, Antonelli M, Gilardi B (2020) Experimental study of braced steel frames subjected to fire after earthquake. 17th World Conference on Earthquake Engineering 17WCEE Sendai.
63. Center for Computational Research, University at Buffalo, 2022. <http://hdl.handle.net/10477/79221>

**Publisher's Note** Springer Nature remains neutral with regard to jurisdictional claims in published maps and institutional affiliations.

Springer Nature or its licensor (e.g. a society or other partner) holds exclusive rights to this article under a publishing agreement with the author(s) or other rightsholder(s); author self-archiving of the accepted manuscript version of this article is solely governed by the terms of such publishing agreement and applicable law.